Achieving Robust Localization in Geometrically Degenerated Tunnels

Weikun Zhen, Sebastian Scherer

***Abstract*—Although many methods have been proposed to localize a robot using onboard sensors in GPS-denied environments, achieving robust localization in *geometrically degenerated* tunnels remains a challenging problem in robot-based inspection tasks. In this work, we first present a novel model to analyze the *localizability* of the prior map at a given location. Then we propose the utilization of a single Ultra-Wideband (UWB) ranging device to compensate for the degeneration of LiDAR based localization inside tunnels. A probabilistic sensor fusion method is developed and demonstrated to achieve real-time robust localization inside a geometrically degenerated tunnel.**

I. Introduction

In this paper, we address the localization problem in robot-based tunnel inspection tasks. Compared with traditional human-based approaches, robots are more flexible and efficient in that it does not require specialized tools to gain mobility, and is able to access places that are dangerous for humans. However, localizing a robot inside tunnels can be difficult even for the state-of-the-art methods due to the darkness and ambiguity inside the tunnel.

To achieve self-localization, LiDAR is more widely used than other sensors due to its long ranging capacity and robustness to low illumination. However, since a LiDAR captures geometry information by scanning the environment, it is more likely to be affected in geometrically degenerated cases. For example, a robot navigating through a long straight tunnel (as seen in Fig. 1 up-left) will not be able to determine its location along the tunnel since the measurements are identical everywhere. We could understand the degeneration with an analogy to a sliding block inside a pipe (see Fig. 1 lower-left). Since there is no contact force restraining the object, its motion along the pipe becomes under-constrained.

To identify geometric degeneration in general environments, a model to predict the localizability is needed. Besides, a theoretical model can also assist in designing new sensing capacity to eliminate degeneration. In this work, we first reformulate the localizability model proposed in [8] to incorporate robot orientation, and then propose the utilization of a UWB ranging device to fully constrain the pose estimation problem. Finally, the UWB ranging information is fused with a rotating 2D LiDAR in a Bayesian filtering framework and it is shown that the localization performance is significantly improved inside a geometrically degenerated tunnel.

The main contribution of this paper can be summarized as: (1) We propose a novel localizability evaluation method that is easy to implement and physically meaningful; (2) We present a localization system which shows that a single ranging device is able to significantly reduce the drifts in a geometrically degenerated tunnel.

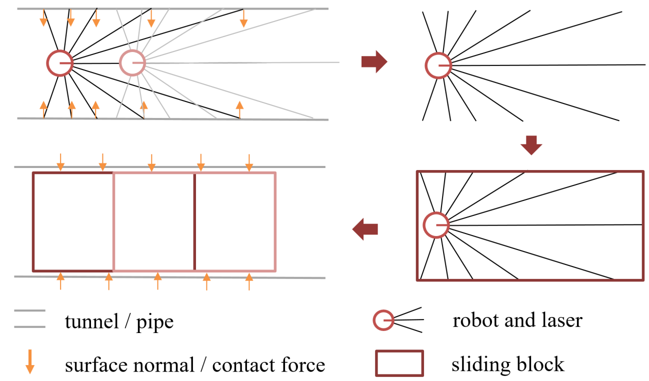

Fig. 1: An analogy between robot navigation inside a tunnel and a sliding block inside a pipe, where the measured surface normals correspond to contact forces.

The structure of this paper is as follows. Section II discusses related work on localizability prediction. Section III describes the proposed localizability model in detail and also introduces the sensor fusion method. Experimental results are presented in Section IV and conclusions are drawn in Section V.

II. Related Work

There are plenty of work modelling the sensor localizability or uncertainty. Perhaps the earliest attempt is from Roy et al. [5] which is also known as *coastal navigation*. Their model is formulated in a probabilistic framework but needs approximations to compute the uncertainty efficiently. Censi et al. [1] derive a lower bound of the uncertainty matrix that ICP algorithms can achieve using Cremar-Rao's bound, which actually inspires the development of our method. Liu et al. [3] provide an numerical implementation of this approach in 2D and a planner is developed to maximize the determinant of the computed information matrix. Zhang et al. [7] propose to use a *degeneracy factor* to characterize geometric degeneration and improve the accuracy of ego-motion estimation in the context of solving an optimization problem. Our previous work [8] describes a simple method that builds an information matrix from 3D normal vectors and use its eigenvalues to measure the localizability. However, it only considers translation and does not provide an explanation for the metric of localizability. Instead of LiDARs, Eudes et al. [2] model the error propagation from image pixels to reconstructed 3D points. And Vega et al. [6] propose a learning based approach to predict uncertainty matrix based on observed features.

Our approach shares a similar idea with [1] and [7] in that the sensitivity of measurements w.r.t. parameters is used to identify degeneration. But we formulate the sensitivity from a constraint set and use a different but physically meaningful metric to evaluate the localizability.

III. Approach

A. The Degeneration of Geometry

The goal of modelling the degeneration of geometry is to develop theoretical tools to identify degeneration in given maps and also gain insights on designing reliable sensing systems. In other words, given the prior map, we would like to answer whether the current measurement from a specific sensor contains enough information to estimate the robot state.

1) Localizability of the LiDAR: First of all, we represent the LiDAR based localization problem as solving a set of constraint equations:

$$\mathcal{C}(\mathbf{x}, \mathbf{R}, \rho_i) = \mathbf{n}_i^T(\mathbf{x} + \mathbf{R}\mathbf{r}_i\rho_i) + d_i = 0 \quad (1)$$

where $(\mathbf{x}, \mathbf{R}) \in (\mathbb{R}^3, SO(3))$ denotes the robot position and orientation, and $i \in \{1, 2, \cdots, m\}$ is the point index in a single laser scan. $(\mathbf{n}_i, d_i) \in (\mathbb{R}^3, \mathbb{R})$ encodes the unit normal vector and distance of the local surface. $\mathbf{r}_i \in \mathbb{R}^3$ is the unit range vector represented in the robot body frame and $\rho_i \in \mathbb{R}$ is the range value. Eqn. 1 describes a simple fact that the scanned points should align with the map when the robot is at the correct location.

Now we evaluate the *strength* of the constraint by measuring the sensitivity of measurements w.r.t. the robot pose. The key observation is that if the robot pose is perturbed slightly but the resulting measurements do not change much, then the constraint is weak. Otherwise, the constraint is strong. Therefore, it is natural to compute the derivative of ρ_i w.r.t. $\mathbf{x}$ and $\mathbf{R}$ as a measure of the sensitivity. Stacking the derivatives computed from all the constraints gives two matrices:

$$\mathbf{F} = \begin{bmatrix} -\frac{\mathbf{n}_1}{\mathbf{n}_1^T\mathbf{r}_1} & \cdots & -\frac{\mathbf{n}_m}{\mathbf{n}_m^T\mathbf{r}_m} \end{bmatrix}^T \quad (2)$$

$$\mathbf{T} = \begin{bmatrix} -\frac{\rho_1\mathbf{r}_1 \times \mathbf{n}_1}{\mathbf{n}_1^T\mathbf{r}_1} & \cdots & -\frac{\rho_m\mathbf{r}_m \times \mathbf{n}_m}{\mathbf{n}_m^T\mathbf{r}_m} \end{bmatrix}^T \quad (3)$$

(see Appendix A for details). We then perform Eigen Decomposition (ED) on the information matrices $\mathbf{F}^T\mathbf{F}$ and $\mathbf{T}^T\mathbf{T}$ and use the eigenvalues to identify the direction of degeneration. Additionally, we project each row in $\mathbf{F}$ and $\mathbf{T}$ into the eigenspace and use the sum of the absolute values as a measure of the localizability in each dimension.

A closer look at $\mathbf{F}$ and $\mathbf{T}$ gives a more natural and intuitive interpretation. As illustrated in Figure 2, we can interpret the position constraints as forces in the direction of $\mathbf{n}_i$ (ignoring the signs) and the orientation constraints as torques in the direction of $\mathbf{r}_i \times \mathbf{n}_i$. Now the $\mathbf{F}$ and $\mathbf{T}$ are collections of wrenches (forces and torques) restraining the translation and rotation of the robot. Aligning with this picture, well-conditioned $\mathbf{F}$ and $\mathbf{T}$ indicate a *frictionless force-closure*, which is a term used in the field of manipulation mechanics

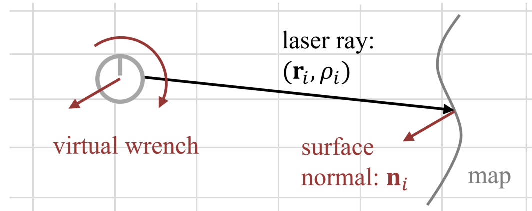

Fig. 2: An illustration of the visual wrench restraining the robot position and orientation.

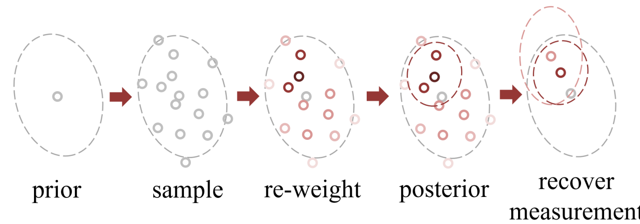

Fig. 3: An illustration of the GPF in 2D. Grey ellipse: uncertainty of prior belief. Dark red ellipse: uncertainty of posterior. Light red ellipse: uncertainty of the recovered pose measurement. The color of particles encodes its weight. Higher weight corresponds to darker color.

to describe a solid grasp of an object, meaning potential motions in all directions are prohibited. The characterization of frictionless force-closure is to check whether the row vectors in $\mathbf{F}$ and $\mathbf{T}$ span the space of $\mathbb{R}^3$ [4]. Thus we interpret the metric of the localizability as the magnitude of accumulated virtual forces and torques gained from the measurements restraining the uncertainty of pose estimation.

2) Localizability of UWB Ranging: The UWB sensor measures the distance from the anchor (attached to the environment) to the target (attached to the robot). Assuming the target is located at the origin of the robot body frame, we get the constraint equation:

$$\mathcal{C}(\mathbf{x}, \mathbf{R}, \gamma) = ||\mathbf{x} - \mathbf{x}_a||^2 - ||\gamma||^2 = 0 \quad (4)$$

where $\mathbf{x}_a \in \mathbb{R}^3$ is the anchor position in the environment and $\gamma \in \mathbb{R}$ is the measured range. Following similar procedures in finding Eqn. 2 and 3, we obtain the force matrix $\mathbf{F}$ for the UWB:

$$\mathbf{F} = \frac{\mathbf{x} - \mathbf{x}_a}{\gamma} \quad (5)$$

(see Appendix B). Again $\mathbf{F}$ can be treated as a collection of unit force in the direction from the anchor to the target. Since the sensor does not provide any information of the orientation, the torque matrix $\mathbf{T}$ is trivially zero.

B. Probabilistic Fusion of LiDAR and UWB

The LiDAR based localization uses an Error State Kalman Filter (ESKF) to estimate robot pose, velocity and IMU biases, where IMU integration is the motion model and scan to grid map matching is the measurement model. We refer readers to our paper [8] for more details.

The fusion of UWB ranges into the filtering framework is achieved using a Gaussian Particle Filter (GPF). Specifically, we first draw a set of particles $\{\mathbf{x}_i | i = 1, 2, \cdots\}$ according to the prior belief computed from the motion model. Then for each particle, we compute a weight using the likelihood function:

$$w_i = \exp\left[-\left(\frac{||\mathbf{x}_i - \mathbf{x}_a|| - \gamma}{\sigma}\right)^2\right] \tag{6}$$

where σ is the ranging noise of the UWB. By computing the weighted mean and covariance of the particle set, we find the posterior belief. With both the prior and posterior in hand, we differentiate them to recover a position measurement. This pose measurement is finally used to update the ESKF. Fig. 3 illustrates the process of handling UWB ranges to recover a position measurement.

IV. Experiments

A. Overview

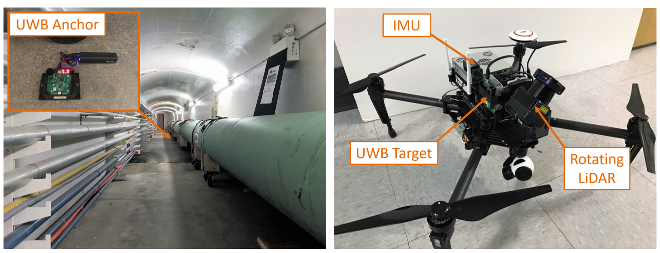

Fig. 4: *Left*: The Smith Hall tunnel at CMU. *Right*: The robot setup used for experiments.

Experiments are carried out inside the Smith Hall tunnel on the campus of CMU. The prior map is acquired offline by registering scans using the ICP method. Fig. 4 shows the tunnel and the robot platform. The tunnel is of size 35m $\times$ 2.4m $\times$ 2.5m ($l \times w \times h$) with pipes on both sides. The robot is a DJI Matrice 100 drone with customized payloads including a rotating Hokuyo LiDAR (40Hz, 30m range), a Microstrain IMU (100Hz) and a Pozyx UWB target board (100Hz, 100m range with clear line-of-sight).

B. Localizability inside the Tunnel

LiDAR localizability is evaluated at 20 evenly sampled places along the tunnel. To simulate the measurement at each place, 4000 points are selected uniformly within the range of 15 meters. The effective range of LiDAR decreases since a number of points has nearly 90° reflection angle. We choose 4000 since that is the amount of downsampled laser points used for localization per unit time length (1 second). The localizability is computed by $l_i = s_i / \sum s_i, \ (i = 1, 2, 3)$, where s is the sum of rows of $\mathbf{F}$ or $\mathbf{T}$ projected into the eigenspace. Note that x-axes of the eigenspace and the body frame is parallel as it is the generated direction. However, that is not necessarily the case for y and z if there is no significant difference of constraint strength. The computation is repeated 10 times with different set of points and results are averaged. Fig. 5 shows a top-down view of the sampled poses and the their localizability. It can be observed that the position and

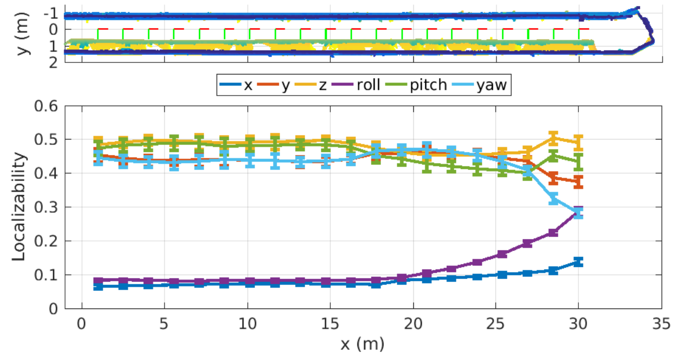

Fig. 5: LiDAR localizability along the tunnel.

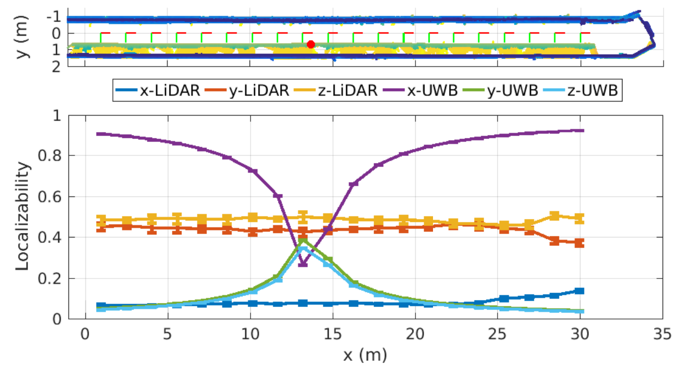

Fig. 6: A comparison of position localizability of the LiDAR and the UWB ranging sensor.

orientation localizability along x-axis is significantly smaller than the other two dimensions. This is because position x is ambiguous along the tunnel except at the right end where a vertical wall exists to restrain the position. Additionally, since the tunnel has an arc ceiling and almost identical width and height, roll angle can not be effectively constrained by LiDAR measurements. Fortunately, the IMU data is fused in localization and it directly measures the orientation.

Considering the UWB, we project the range measurements into the fore-mentioned eigenspace, evaluate the localizability, and compare that with the LiDAR (see Fig. 6). It is easy to observe that the UWB compensates the LiDAR localizability along x-axis. However, we observe a decrease of localizability in x near the anchor (red dot). This is a singular point where only position y is measured. Theoretically, additional anchors may be needed to solve this issue. In practice, this does not cause failure, since the time of being under-constrained is short.

C. Tunnel Localization Test

The localization test is conducted by manually flying the robot from the map origin to the other end of the tunnel. The UWB anchor board is installed a priori and its location is measured in the point cloud map. In this experiment, we control the usage of UWB ranging data and compare the localization performance. When the UWB ranging is disabled, the localization starts to drift shortly after the robot takes off. However, when

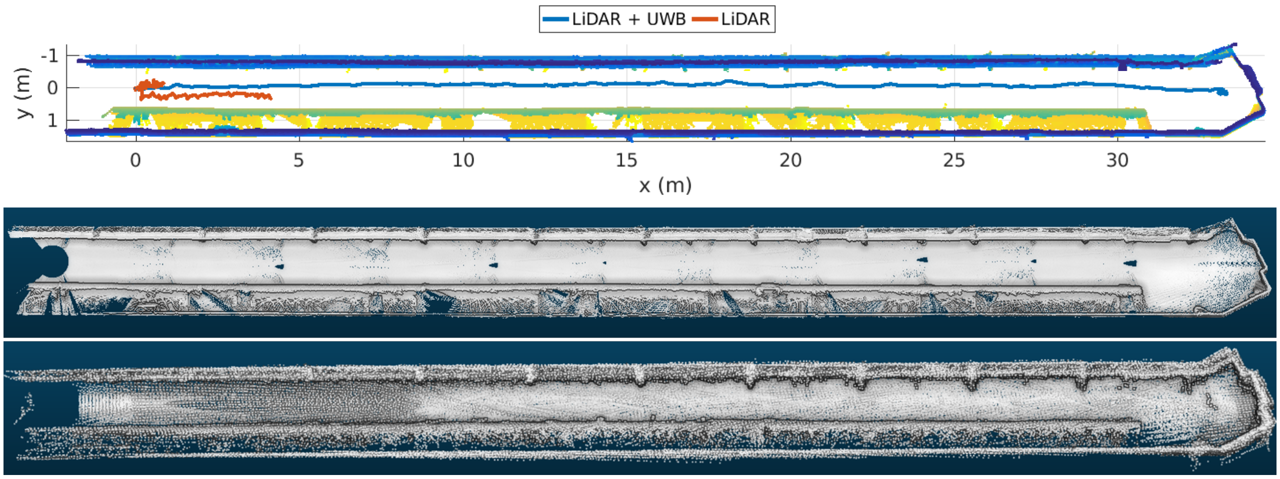

Fig. 7: *Up*: A comparison of estimated trajectories with/without the UWB ranging. *Middle*: The groundtruth map built by manually match multiple local scans. *Bottom*: The reconstructed map by assembling laser scans with estimated poses.

the UWB ranging information is fused with LiDAR, the robot is able to successfully localize itself throughout the whole test. Fig. 7 shows the estimated trajectories, the prior map and the reconstructed map. Since the localization accuracy is difficult to be measured without a motion capture system, we use the reconstructed map to qualitatively evaluate estimation accuracy. Although the reconstructed map shows larger noise than the prior map, the side structures are recovered, indicating correct localization.

V. Conclusion

This paper presents a novel geometric degeneration modelling method that encodes the sensitivity of measurements w.r.t. robot poses. We find an analogy between the force-closure characterization and our method, which helps to explain the physical meaning of the localizability. Additionaly, it is shown that the LiDAR and the UWB ranging sensor are complementary in terms of localizability and the presented fusion method is demonstrated to allow for robust localization inside real geometrically degenerated tunnels.

There are several directions for future work. Firstly, the constraint model of a localization problem is potentially generalizable to other sensors such as cameras. Second, it is still not clear how to compute the total localizability when multiple sensors of different modalities exist. In our experience, directly compositing constraints does not give reasonable results since sensor information may be redundant and the data comes at different time and frequency. Finally, the proposed fusion algorithm will be deployed in larger environments, where multiple UWB anchors may be required.

Appendix A

Without losing generality, we could always define the map frame to align with the robot body frame. In this way, $(\mathbf{x}, \mathbf{R})$ are small and can be treated as perturbations. Therefore the problem is reduced to evaluate how sensitive is ρ_i w.r.t. the perturbations $(\mathbf{x}, \mathbf{R})$. This assumption allows using the small angle approximation $\mathbf{R} \approx \mathbf{I} + [\boldsymbol{\theta}]_\times$ to find the linearized constraint:

$$\begin{aligned} \bar{\mathcal{C}}(\mathbf{x}, \boldsymbol{\theta}, \rho_i) =& \mathbf{n}_i^T(\mathbf{x} + (\mathbf{I} + [\boldsymbol{\theta}]_\times)\mathbf{r}_i\rho_i) + d_i \\ =& \mathbf{n}_i^T\mathbf{x} + \mathbf{n}_i^T\mathbf{r}_i\rho_i + \mathbf{n}_i^T[\boldsymbol{\theta}]_\times\mathbf{r}_i\rho_i + d_i \\ =& \mathbf{n}_i^T\mathbf{x} + \mathbf{n}_i^T\mathbf{r}_i\rho_i - \mathbf{n}_i^T[\mathbf{r}_i]_\times\boldsymbol{\theta}\rho_i + d_i \end{aligned} \tag{7}$$

Then based on the Implicit Function Theorem (IFT), we have

$$\frac{\partial \bar{\mathcal{C}}}{\partial \mathbf{x}}\mathrm{d}\mathbf{x} + \frac{\partial \bar{\mathcal{C}}}{\partial \rho_i}\mathrm{d}\rho_i = 0, \quad \frac{\partial \bar{\mathcal{C}}}{\partial \boldsymbol{\theta}}\mathrm{d}\boldsymbol{\theta} + \frac{\partial \bar{\mathcal{C}}}{\partial \rho_i}\mathrm{d}\rho_i = 0 \tag{8}$$

which implies

$$\begin{aligned} \frac{\mathrm{d}\rho_i}{\mathrm{d}\mathbf{x}} &= -\left(\frac{\partial \bar{\mathcal{C}}}{\partial \mathbf{x}}\right)\left(\frac{\partial \bar{\mathcal{C}}}{\partial \rho_i}\right)^{-1} = -\frac{\mathbf{n}_i^T}{\mathbf{n}_i^T\mathbf{r}_i} \\ \frac{\mathrm{d}\rho_i}{\mathrm{d}\boldsymbol{\theta}} &= -\left(\frac{\partial \bar{\mathcal{C}}}{\partial \boldsymbol{\theta}}\right)\left(\frac{\partial \bar{\mathcal{C}}}{\partial \rho_i}\right)^{-1} = -\frac{(\rho_i\mathbf{r}_i \times \mathbf{n}_i)^T}{\mathbf{n}_i^T\mathbf{r}_i} \end{aligned} \tag{9}$$

The derivatives are then stacked into matrix $\mathbf{F}$ and $\mathbf{T}$.

Appendix B

Similarly, based on the IFT, we have

$$\frac{\partial \mathcal{C}}{\partial \mathbf{x}}\mathrm{d}\mathbf{x} + \frac{\partial \mathcal{C}}{\partial \gamma}\mathrm{d}\gamma = 0 \tag{10}$$

which implies

$$\frac{\mathrm{d}\gamma}{\mathrm{d}\mathbf{x}} = -\left(\frac{\partial \mathcal{C}}{\partial \mathbf{x}}\right)\left(\frac{\partial \mathcal{C}}{\partial \gamma}\right)^{-1} = \frac{\mathbf{x} - \mathbf{x}_a}{\gamma} \tag{11}$$

References

[1] Andrea Censi. On achievable accuracy for range-finder localization. In *Proceedings 2007 IEEE International Conference on Robotics and Automation*, pages 4170–4175. IEEE, 2007.

[2] Alexandre Eudes and Maxime Lhuillier. Error propagations for local bundle adjustment. In *Computer Vision and*

Pattern Recognition, 2009. CVPR 2009. IEEE Conference on, pages 2411–2418. IEEE, 2009.

[3] Zhe Liu, Weidong Chen, Yong Wang, and Jingchuan Wang. Localizability estimation for mobile robots based on probabilistic grid map and its applications to localization. In *Multisensor Fusion and Integration for Intelligent Systems (MFI), 2012 IEEE Conference on*, pages 46–51. IEEE, 2012.

[4] Richard M Murray. *A mathematical introduction to robotic manipulation*. CRC press, 2017.

[5] Nicholas Roy and Sebastian Thrun. Coastal navigation with mobile robots. In *Advances in Neural Information Processing Systems*, pages 1043–1049, 2000.

[6] William Vega-Brown, Abraham Bachrach, Adam Bry, Jonathan Kelly, and Nicholas Roy. Cello: A fast algorithm for covariance estimation. In *Robotics and Automation (ICRA), 2013 IEEE International Conference on*, pages 3160–3167. IEEE, 2013.

[7] Ji Zhang, Michael Kaess, and Sanjiv Singh. On degeneracy of optimization-based state estimation problems. In *Robotics and Automation (ICRA), 2016 IEEE International Conference on*, pages 809–816. IEEE, 2016.

[8] Weikun Zhen, Sam Zeng, and Sebastian Scherer. Robust localization and localizability estimation with a rotating laser scanner. In *2017 IEEE International Conference on Robotics and Automation (ICRA)*, Singapore, Singapore, 2017. IEEE.